ISSN: 2579-5821 (Print)
ISSN: 2579-5546 (Online)
URL address: http://journal.unhas.ac.id/index.php/geocelebes
DOI: 10.70561/geocelebes.v9i2.46445

Jurnal Geocelebes Vol. 9 No. 2, October 2025, 189 – 212

Comparative Analysis of SARIMA, FFNN, and Hybrid Models for Sea Surface Temperature Prediction at Enggano Island (2018–2024)

Raditya Janaloka Natisharevi, Jose Rizal*, Firdaus, Pepi Novianti, Wina Ayu Lestari

Department of Statistics, Faculty of Mathematics and Natural Science, University of Bengkulu, Bengkulu 38371, Indonesia

*Corresponding author. Email: jrizal04@unib.ac.id

Manuscript received: 21 August 2025; Received in revised form: 13 October 2025; Accepted: 15 October 2025

Abstract

Sea Surface Temperature (SST) is a key oceanographic variable that influences fish distribution and the livelihoods of coastal communities. On Enggano Island, where most residents rely on fishing, SST is critical for identifying optimal fishing grounds due to limited accessibility and high operational costs. Accurate modeling and forecasting of SST are therefore essential for effective fisheries management and sustainable resource use. This study analyzes and predicts monthly SST patterns in Enggano Island using Seasonal Autoregressive Integrated Moving Average (SARIMA), Feed Forward Neural Network (FFNN), and Hybrid SARIMA-FFNN models. SARIMA effectively captures linear trends and seasonal variations but struggles with nonlinear dynamics and requires statistical assumptions. Conversely, FFNN models nonlinear relationships without such assumptions but is less efficient in representing linear and seasonal structures. The hybrid SARIMA-FFNN combines the strengths of both approaches, integrating linear-seasonal accuracy with nonlinear adaptability. Monthly SST data from January 2018 to December 2024, covering northern, eastern, southern, and western regions of Enggano Island, were analyzed. Results show that all models achieved high predictive accuracy, with MAPE values below 10%. Based on RMSE, FFNN outperformed the other models across all regions (north: 1.173, east: 0.999, south: 1.245, west: 1.049), confirming FFNN as the most accurate model for SST prediction. Predicted SST values across the four regions exhibited only minor differences, offering fishermen flexibility in selecting fishing grounds. Sustainable fishing strategies should also consider species-specific temperature preferences and other ecological factors influencing fish distribution.

Keywords: Enggano Island; FFNN; Hybrid SARIMA-FFNN; SARIMA; Sea Surface Temperature.

Citation: Natisharevi, R. J., Rizal, J., Firdaus, F., Novianti, P., & Lestari, W. A. (2025). Comparative Analysis of SARIMA, FFNN, and Hybrid Models for Sea Surface Temperature Prediction at Enggano Island (2018–2024). *Jurnal Geocelebes*, 9(2):189–212, doi: 10.70561/geocelebes.v9i2.46445

Introduction

Oceanography is the scientific discipline that studies various dynamic and physical processes in seawater (Kambey et al., 2023). One of the important variables in oceanography is sea surface temperature (SST), which influences fish distribution (Rifai, 2023). This factor is particularly crucial for the residents of Enggano Island, the majority of whom work as fishermen (Silsia et al., 2019). Enggano Island is one of the outermost islands in Bengkulu Province, relatively remote with very limited access, requiring approximately 12 hours of sea travel to reach (Sari, 2020). Such limited accessibility affects the high price of fuel oil, which serves as the primary energy source for fishing vessels, since fuel is supplied in small quantities from Bengkulu City via sea transportation (Silsia et al., 2019). This situation poses a challenge for Enggano fishermen, who generally rely only on experience in determining fishing locations. As a result, fishermen often set sail without certainty regarding optimal fishing grounds, which may lead to increased operational costs or low catch yields (Baharudin et al., 2022). One solution to the problem of fishing ground determination is predicting

SST, with the expectation that it can provide insights into optimal fishing locations (Shabrina et al., 2017).

SST exhibits seasonal patterns influenced by meteorological conditions (Hastuti et al., 2024). Therefore, one of the appropriate models to apply is the Seasonal Autoregressive Integrated Moving Average (SARIMA). This model represents that the current observation is affected by previous observations and prediction errors in both regular and seasonal periods. However, SARIMA has certain limitations, particularly the statistical assumptions that must be satisfied, such as data stationarity and the white noise assumption. In addition, SARIMA is unable to capture nonlinear patterns in the data (Susila et al., 2023). These limitations can be addressed through the application of Neural Networks (NN).

NN do not require statistical assumptions in modeling and are capable of learning nonlinear patterns in data through their network structures and activation functions (Zhang, 2003). NN are artificial representations of the human brain that continuously attempt to simulate the learning mechanisms of the human mind (Septiana & Bangun, 2023). Various network architectures exist within Neural Networks, one of which is the Feed Forward Neural Network (FFNN). The principle of FFNN is to transmit information forward from the input layer to the hidden layer and then to the output layer, without the presence of loops (Aminy & Walid, 2022). Although the flow of information is unidirectional, the weights in FFNN are updated using the backpropagation algorithm to produce more accurate predictions. Nevertheless, FFNN tends to be less effective in capturing linear and seasonal structures in time series data (Fadhlia et al., 2024).

Considering these complementary strengths and weaknesses, the Hybrid SARIMA-FFNN model integrates both approaches to leverage their advantages. In this framework, the residuals from the SARIMA model, which represent the nonlinear components, are used as inputs for the FFNN to capture nonlinear dynamics. The outputs from the FFNN are then combined with the SARIMA predictions to produce the final forecast, thereby enhancing accuracy in complex time series such as SST (Fadhlia et al., 2024). Since SST can exhibit linear patterns, nonlinear dynamics, or a combination of both due to interactions between seasonal cycles, ocean currents, and meteorological factors, it is important to systematically compare SARIMA, FFNN, and hybrid approaches to determine which method is most suitable for different data characteristics, avoiding models that are either too simple or unnecessarily complex.

Several studies have been conducted on the modeling and prediction of sea surface temperature (SST). Syahrin et al. (2024) utilized the NeuralProphet model to forecast SST. However, this model does not specifically accommodate the seasonal patterns present in SST data. Meanwhile, Hisyam et al. (2025) applied the SARIMA approach to predict SST, which is effective in representing seasonal components. Nevertheless, this model is less capable of capturing nonlinear patterns that may arise in SST data. Based on these studies, it is evident that each model has its strengths and limitations. Consequently, a research gap remains in the development of methods that can integrate the advantages of both approaches for SST forecasting. In addition, studies on SST prediction in Bengkulu Province, particularly in Enggano Island, are still very limited.

Therefore, this study aims to address the existing research gap by modeling sea surface temperature (SST) in Enggano Island using SARIMA, FFNN, and Hybrid SARIMA-FFNN approaches. In addition to developing these models, the study also seeks to evaluate the performance of all three approaches, with the expectation of providing new insights into the most

effective model for supporting improved SST prediction accuracy.

Materials and Methods

Data Type and Sources

This study utilized secondary data, which was obtained from Giovanni, a free web-based system from NASA accessible at https://giovanni.gsfc.nasa.gov/giovanni. The data used was monthly SST observations, recorded from January 2018 to December 2024. The collected data was of the time series area average type with several specifications. The SST data was specifically taken at nighttime to avoid measurement bias caused by the reflection of solar radiation. This choice is also relevant as it aligns with the common practice of local fishermen, who typically go out to sea at night to maximize their catch. Furthermore, a 4 km spatial resolution was used to obtain a more detailed and accurate view of the research area, and an 11-micron spectral resolution was chosen because it represents the most reliable wavelength for measuring SST. This data covers four distinct observation locations: the northern, southern, western, and eastern parts of Enggano Island. An illustration of these observation areas is presented in Figure 1.

Figure 1. Illustration of observation area.

Figure 1 illustrates the observation area. The specific details of the observation locations are provided by the following coordinates:

1. East: 05º11'S – 05º32'S and 101º50'E – 102º05'E.
2. North: 05º11'S – 05º17'S and 101º59'E – 102º29'E.
3. West: 05º11'S – 05º32'S and 102º23'E – 102º29'E.
4. South: 05º29'S – 05º35'S and 101º59'E – 102º29'E.

For modeling purposes, the data were partitioned into 72 data points were used for training, and the remaining 12 points were used for testing. This partition preserves the full annual cycle in the training data, which is important for capturing seasonal patterns in SST. The selection of the 72:12 split was guided by preliminary spectral analysis, ensuring that the strongest seasonal components were retained in the training set while allowing for reliable out-of-sample evaluation.

Data Cleaning

Data cleaning is the process of identifying and correcting incorrect data (Azmi et al., 2023). In this study, the data cleaning process focuses on addressing the issue of

missing values. Since this research utilizes time series data, which requires complete and sequential observations for proper analysis (Wei, 2006), data imputation is considered the most appropriate approach.

If missing data are found at the beginning or end of the dataset, imputation will be carried out using linear extrapolation according to Equation 1 (Pangruruk & Barus, 2022).

$$Z_t = \begin{cases} Z_{t1} + \frac{Z_{t2}-Z_{t1}}{t_2-t_1}(t-t_1), \text{for } t < t_1 \\ Z_{t2} + \frac{Z_{t2}-Z_{t1}}{t_2-t_1}(t-t_2), \text{for } t < t_2 \end{cases} \quad (1)$$

Meanwhile, if missing data occur between two observation points, imputation will be performed using linear interpolation according to Equation 2 (Pangruruk & Barus, 2022).

$$Z_t = Z_{t1} + \frac{Z_{t2} - Z_{t1}}{t_2 - t_1}(t - t_1) \quad (2)$$

where Z_{t1} represents the second-to-last known value and Z_{t2} represents the last known value.

Seasonal Pattern Testing

Seasonal patterns can be identified using spectral regression. Spectral regression is a technique useful for detecting hidden periodicities in data (Wei, 2006). The first step in this testing involves representing the data using a Fourier equation, as shown in Equation 3 (Wei, 2006).

$$Z_t = \sum_{m=0}^{\left[\frac{n}{2}\right]} (a_m \cos \omega_m t + b_m \sin \omega_m t) \quad (3)$$

where $m = 0,1, \dots, [\frac{n}{2}]$ represents the frequency components of ω_m dan $\omega_m = \frac{2\pi m}{n}$ denotes the Fourier frequency.

Next, the Fourier coefficients are calculated using Equations 4 to 6 (Wei, 2006).

1. For $m = 0$ dan $m = \frac{n}{2}$ if n even

$$a_m = \frac{1}{n}\sum_{t=1}^{n} Z_t \cos \omega_m t \quad (4)$$

2. For $m = 1,2, \dots, \left[\frac{n-1}{2}\right]$

$$a_m = \frac{2}{n}\sum_{t=1}^{n} Z_t \cos \omega_m t \quad (5)$$

$$b_m = \frac{2}{n}\sum_{t=1}^{n} Z_t \sin \omega_m t \quad (6)$$

Next, the ordinate values are calculated using Equation 7.

$$I(\omega_m) = \begin{cases} na_0^2, m = 0, \\ \frac{n}{2}(a_m^2 + b_m^2), m = 1, \dots, \left[\frac{n-1}{2}\right], \\ na_{n/2}^2, m = \frac{n}{2} \text{ when } n \text{ even.} \end{cases} \quad (7)$$

After obtaining the ordinate values that reflect the strength of the seasonal components, the highest ordinate value is then tested using a hypothesis test. The hypotheses are:
$H_0: a_m = b_m = 0$ (not influenced by seasonal components)
$H_1: a_m \neq 0$ atau $b_m \neq 0$ (influenced by seasonal components).

The test statistic is calculated using Equation 8 (Wei, 2006).

$$T = \frac{I^{(m)}(\omega_{(m)})}{\Sigma_{m=1}^{\left[\frac{n}{2}\right]} I(\omega_m)}. \quad (8)$$

If the value of $T > g_\alpha$, then H_0 is rejected, it means that seasonal components influence the data.

Data Stationarity

A process $\{Z_t\}$ is said to be stationary if it satisfies the following conditions (Wei, 2006):

1. $E(Z_t) = \mu$, constant for all t.
2. $Var(Z_t) = E(Z_t - \mu)^2 = \sigma^2$, constant for all t.
3. $Cov(Z_t, Z_{t-k}) = \gamma_{t,t-k} = \gamma_k$, constant for all t.

Data are considered to meet the stationarity criteria if both the variance and mean remain constant over time. The assumption of stationarity in variance is considered satisfied if the value of λ is equal to or close

to one. If this assumption is not met, it can be addressed using the Box-Cox transformation, as shown in Equation 9 (Cryer & Chan, 2008).

$$Z_t(\lambda) = \begin{cases} \dfrac{Z_t^{\lambda} - 1}{\lambda}, (\lambda \neq 0) \\ ln\, Z_t, (\lambda = 0). \end{cases} \quad (9)$$

The stationarity assumption of the mean can be tested using the Augmented Dickey-Fuller (ADF) test, with $H_0 : \psi = 0$ (The data are non-stationary in mean) dan $H_1 : \psi < 0$ (The data are stationary in mean). The test statistic used is as follows (Cryer & Chan, 2008):

$$\tau = \frac{\hat{\psi}}{SE(\hat{\psi})}. \quad (10)$$

If the test statistic value is obtained $\tau < DF_{(\alpha)}$ or $P_{value}(\tau) < \alpha$, then H_0 is rejected. Here, the value of τ is obtained from the calculation in Equation 10, and $DF_{(\alpha)}$ represents the critical value taken from the Dickey-Fuller distribution table at the chosen significance level. Rejection of H_0 indicates that the tested data are stationary in mean. If the data do not yet satisfy mean stationarity, it can be addressed using differencing, either non-seasonal ($\Delta^d Z_t = (1-B)^d Z_t$) or seasonal ($\Delta^s Z_t = (1-B)^s Z_t$).

Autocorrelation Function (ACF)

The ACF is a function used to describe the correlation between Z_t and Z_{t+k} separated by a lag of k time units. The ACF estimation is expressed in Equation 11 (Wei, 2006).

$$\hat{\rho}_k = \frac{\hat{\gamma}_k}{\hat{\gamma}_0} = \frac{\Sigma_{t=1}^{n-k}(z_t - \bar{z})(z_{t+k} - \bar{z})}{\Sigma_{t=1}^{n}(z_t - \bar{z})^2} \quad (11)$$

Partial Autocorrelation Function (PACF)

The PACF is a function used to measure the direct strength of the relationship between Z_t and Z_{t+k}, assuming that the effects of the intervening lags $1, 2, 3, \ldots, k-1$ are removed. The PACF can be estimated using Equation 12 (Wei, 2006).

$$\hat{\phi}_{k,k} = \frac{\hat{\rho}_k - \Sigma_{j=1}^{k-1}\hat{\phi}_{k-1,j}\,\hat{\rho}_{k-j}}{1 - \Sigma_{j=1}^{k-1}\hat{\phi}_{k-1,j}\,\hat{\rho}_j} \quad (12)$$

Seasonal Autoregressive Integrated Moving Average (SARIMA)

SARIMA is a model that represents the dependence of the current observation on both previous observations and predictions, as well as on observations from previous seasonal periods. Mathematically, the SARIMA model is expressed in Equation 13 (Wei, 2006).

$$\phi_p(B)\Phi_P(B^S)(1-B)^d\,(1-B^S)^D\,Z_t = \theta_q(B)\,\Theta_Q(B^S)\,e_t \quad (13)$$

SARIMA Steps

SARIMA modeling can be carried out through several steps, as follows:

1. Model identification

ACF and PACF plots, which exhibit characteristics as shown in Table 1, can identify the SARIMA model.

Table 1. Characteristics of ACF & PACF plots (Wei, 2006).

Model	ACF	PACF
AR(p)	Decays exponentially	Cuts off after lag p
MA(q)	Cuts off after lag q	Decays exponentially
AR(P)^S	Decays exponentially at lag lag kS	Cuts off after lag PS
MA(Q)^S	Cuts off after lag QS	Decays exponentially at lag lag kS

2. Parameter estimation method

The parameters of the SARIMA model can be estimated using the Maximum Likelihood Estimation (MLE) approach. MLE is a method of estimation based on the distribution that maximizes the likelihood function.

The general steps in parameter estimation using MLE include identifying the probability density function (PDF) of the data, constructing the likelihood function, transforming it into the log-likelihood, taking the first derivatives to find the parameter values that maximize the log-likelihood, and verifying that these estimates indeed correspond to a maximum by examining the second derivatives.

3. Parameter significance

The significance of the SARIMA model parameters can be tested using the hypothesis test. The hypotheses are:
$H_0: \beta_i = 0$ (significant parameters)
$H_1: \beta_i \neq 0$ (insignificant parameters).

The test statistic as shown in Equation 14 (Wei, 2006).

$$Z = \frac{\hat{\beta}_i}{SE(\hat{\beta}_i)}. \quad (14)$$

If the test statistic value is obtained $|Z| > Z_{\frac{a}{2}}$ or $P_{value}(Z) < \alpha$, this indicates that the parameter is significant.

4. Model diagnostics

The process of verifying that the model is correctly specified is called model diagnostics. Model diagnostics consist of two testing stages: testing the assumption of autocorrelation in the errors and testing the normality of the errors (Wei, 2006). The assumption of autocorrelation in the errors is tested using the Ljung-Box test, with the test statistic $Q = n(n+2)\sum_{k=1}^{K} \frac{\hat{\rho}_k^2}{n-k}$. The normality assumption of the errors is tested using the Kolmogorov-Smirnov (KS) test, with the test statistic defined as $D_{KS} = \sup|F_n(x) - F_0(x)|$. Both assumptions, autocorrelation and normality of the residuals, are considered satisfied if the test statistic value is greater than the critical value, or if the $P_{value} < \alpha$. Meeting these assumptions indicates that the model is correctly specified and suitable for prediction purposes.

5. Selection of the optimal SARIMA model

According to Cryer & Chan (2008), models developed using the Box-Jenkins approach, such as SARIMA, can be compared and evaluated to select the optimal model from several candidate models. In this study, the optimal SARIMA model was chosen based on the lowest values of the Akaike Information Criterion (AIC) and Bayesian Information Criterion (BIC). The AIC and BIC values can be calculated using Equations 15 and 16 (Zhang & Meng, 2023).

$$\text{AIC} = -2\ln(L) + 2I. \quad (15)$$
$$\text{BIC} = -2\ln(L) + I\ln(n). \quad (16)$$

where I denotes the number of parameters in the model and L refers to the maximum value of the likelihood function.

Data Preprocessing

This process represents the initial stage used for network training in the FFNN model. Its purpose is to select the input values to be used, where the input values consist of past observations (Zhang, 2003). In the input layer of the FFNN, the input neurons are derived from a set of variables constructed from the time series data. The following function expresses these variables (Zhang, 2003):

$$Z_t = (X_1, X_2, \ldots, X_I) \quad (17)$$

where $X_i = Z_{t-i}$, $i = 1,2,\ldots,I$, and $t = 1,2,\ldots,n$. This means that each input neuron X_i represents the value of the time series Z at lag i. In other words, the FFNN uses the past I observations of the series as input to predict the current value Z_t.

Data Normalization

Data normalization is the process of rescaling data prior to the learning process, aimed at ensuring that the data can be processed in accordance with the applied activation function (Permana & Salisah, 2022). In this study, min-max scaling normalization was employed, as shown in Equation 18 (Izonin et al., 2022).

$$Z_t' = \frac{Z_t - Z_{min}}{Z_{\max} - Z_{min}}(D - C) + C \quad (18)$$

where D represents the upper range and C represents the lower range of the desired output.

Activation Function

The activation function determines each neuron's output. It operates by transforming the total input received by a neuron into an output that is forwarded to the subsequent neuron. This study employed the binary sigmoid activation function, as it is easily differentiable and does not decrease monotonically. The binary sigmoid activation function is mathematically expressed as shown in Equation 19 (Kurniasari et al., 2023).

$$f(x) = \frac{1}{1 + e^{-x'}} \quad (19)$$

where

$$f'(x) = f(x)\,(1 - f(x)) \quad (20)$$

Equation 20 is the derivative of Equation 19, which will be used to calculate error information in the backpropagation algorithm.

Learning Rate

The training parameter used to control the speed of weight updates in the network is called the learning rate. There is no strict rule for determining the learning rate value; however, it must lie between 0 and 1. A higher learning rate accelerates the training process, but it may also reduce the accuracy of the network's results (Kurniasari et al., 2023).

Weight Initialization

The strength of connections is determined by values called weights. At the initial stage of training, weights are first initialized with small random numbers. Weight initialization in neural networks does not follow a fixed rule, and various methods can be applied. However, based on general heuristics, biases can be initialized to 0, and weights can be generated from a uniform distribution $U\left[-\frac{1}{\sqrt{n}}, \frac{1}{\sqrt{n}}\right]$, where n is the number of neurons in the previous layer (Glorot & Bengio, 2010). After initializing the weights and biases, the network undergoes training, during which the weights are updated to obtain optimal values and produce accurate outputs.

Feed Forward Neural Network (FFNN)

The FFNN is a network architecture capable of handling nonlinear patterns. It consists of three main layers: the input layer, the hidden layer, and the output layer (Ichwan & Alfarisyi, 2024). The input layer feeds data into the network, the hidden layer processes data from the input layer, and the output layer generates outputs based on the provided inputs. Figure 2 illustrates the architecture of the FFNN.

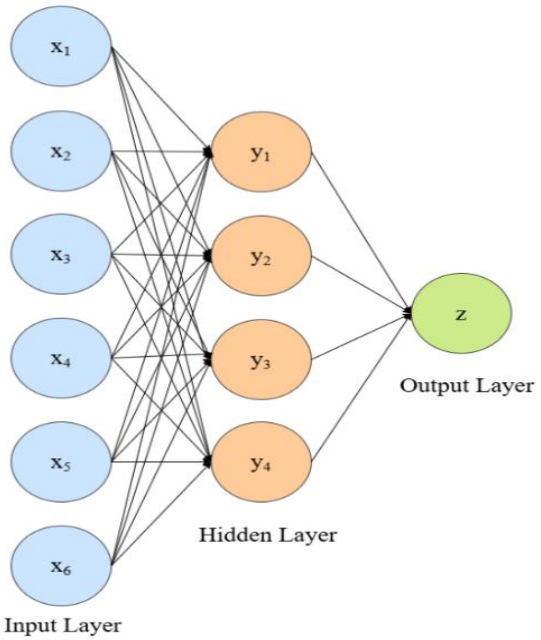

Figure 2. FFNN architecture (Modified from Alrowais et al., 2023).

The principle of the FFNN shown in Figure 2 is the forward flow of information from the input layer to the hidden layer and then to the output layer, without any loops (Aminy & Walid, 2022). The blue circles representing the input neurons process the preprocessed data. This information is then passed to the hidden layer, where the orange circles (hidden neurons) process it through a combination of

weights and activation functions. The output layer, which consists of green neurons, then shows the final output or prediction based on the network's processing. Although the information flows only forward, the weights in the FFNN are updated using the backpropagation algorithm to produce more accurate predictions.

Backpropagation

Backpropagation functions to adjust the weights of all neurons. The process involves several stages: feedforward, backpropagation, and weight and bias updates (Li, 2024). The stages of backpropagation are as follows, and all equations presented in this stage refer to (Wulandari & Novita, 2024):

1. Feedforward
   a. Each input neuron ($X_i, i = 1, 2, , I$) receives an input signal x_i moreover, sends it to the hidden layer.
   b. The weighted sum of signals for each hidden neuron ($Y_h, h = 1, 2, , H$) is calculated as $y_{in_h} = v_{0h} + \sum_{i=1}^{I} x_i v_{ih}$.
      The output signal is then computed using the binary sigmoid activation function $y_h = f(y\_in_h) = \frac{1}{1+e^{-y\_in_h}}$.
   c. The weighted sum of signals for each output unit ($Z_r, r = 1, 2, , R$) is calculated as $z_{in_r} = w_{or} + \sum_{h=1}^{H} y_h w_{hr}$.
      The activation function is applied to produce the output $z_r = f(z\_in_r) = \frac{1}{1+e^{-z\_in_r}}$.

2. Backpropagation
   a. Each output neuron ($Z_r, r = 1, 2, \dots, R$) receives the target pattern corresponding to the learning input and computes the error $\delta_r = (k_r - \hat{z}_r) f'(z_{in_r})$. The weights w_{hr} and bias w_{0r} are then updated using the learning rate α: $\Delta w_{hr} = \alpha \delta_r y_h$ dan $\Delta w_{0r} = \alpha \delta_r$. The δ_r is propagated backward to the previous layer.
   b. Each hidden neuron ($Y_h, h = 1, 2, \dots, H$) computes the sum of delta inputs from the upper layer: $\delta_{in_h} = \sum_{r=1}^{R} \delta_r w_{hr}$. To obtain the error information, this value is multiplied by the derivative of the activation function: $\delta_h = (\delta_{in_h}) f'(y_{in_h})$.
   c. The weights v_{ih} and bias v_{0h} are updated using $\Delta v_{ih} = \alpha \delta_h x_i$ dan $\Delta v_{0h} = \alpha \delta_h$.

3. Weight and bias update
   a. Each output neuron ($Z_r, r = 1, 2, , R$) updates its weights and biases: $w_{hr}(\text{baru}) = w_{hr}(\text{lama}) + \Delta w_{hr}$.
   b. The weights and biases of each hidden neuron ($Y_h = 1, 2, , H$) are updated: $v_{ih}(\text{baru}) = v_{ih}(\text{lama}) + \Delta v_{ih}$.
   c. The stopping condition is checked. The learning process can be terminated if the error $|k_r - z_r| \leq$ *threshold*). In the *neuralnet() package,* the stopping condition is met when the threshold is *reached threshold ≤ threshold.*

The relationship between the output (Z_t) and inputs ($Z_{t-1}, Z_{t-2}, , Z_{t-I}$) is represented by Equation 21 (Zhang, 2003):

$$Z_t = f\left(w_0 + \Sigma_{h=1}^{H} w_h \, f\left(v_{0h} + \Sigma_{i=1}^{I} v_{ih} Z_{t-i}\right)\right) + \varepsilon_t \quad (21)$$

Hybrid SARIMA-FFNN

The Hybrid SARIMA-FFNN model is a combination of linear and nonlinear models, designed to improve prediction accuracy. The working mechanism of the Hybrid SARIMA-FFNN model involves using the errors (nonlinear components) from the SARIMA model as input data, which the FFNN then processes to address nonlinear patterns. The output of the FFNN (nonlinear component) is subsequently

added to the SARIMA model output (linear component). This modeling approach is represented by Equation 22 (Zhang, 2003).

$$Z_t = Z_t^{(L)} + Z_t^{(NL)} + \varepsilon_t. \quad (22)$$

Selection of the Optimal Method

The optimal method was determined based on the calculation of Root Mean Square Error (RMSE) and Mean Absolute Percentage Error (MAPE) on the testing data predictions. The dataset was divided into 72 points for training and 12 points for testing to preserve the full annual cycle, ensuring that seasonal patterns in SST are captured while allowing reliable evaluation of predictive performance. The best-performing model is the one with the lowest RMSE value. The formulas for calculating RMSE and MAPE on the testing data are as follows (Chicco et al., 2021):

$$\text{RMSE}_{test} = \sqrt{\frac{\sum_{t=n_{train}+1}^{n_{test}} \left(\hat{Z}_t - Z_t\right)^2}{n_{test} - n_{train}}} \quad (22)$$

$$\text{MAPE}_{test} = \frac{1}{n_{test}-n_{train}} \sum_{t=n_{train}+1}^{n_{test}} \left|\frac{Z_t - \hat{Z}_t}{Z_t}\right| \times 100\%. \quad (23)$$

The evaluation of MAPE values can be classified based on the accuracy level of the predictions (Puteri, 2023). Table 2 presents the classification of the MAPE evaluation.

Table 2. Classification of MAPE values (Puteri, 2023).

MAPE Value	Prediction Accuracy Classification
< 10%	Very high
10 – 20%	High
20 - 50%	Moderate
> 50%	Poor

Results and Discussion

Data Cleaning

Based on the data collected across all locations, there were ten missing data points, with two occurring at the beginning of the dataset and eight occurring between two valid observations. One possible cause of the missing data is atmospheric obstructions, such as thick clouds, which prevent the satellite sensors from accurately measuring SST, resulting in data that are either unrecorded or deemed not to meet NASA's data quality standards. To ensure a complete dataset for modeling and avoid biases in the analysis, missing values were imputed using interpolation or extrapolation methods. The distribution of missing data and the results of data imputation are presented in Table 3.

Table 3. Distribution and imputation results of the data.

t	North	East	South	West
1	**26.516**	**26.832**	28.061	27.878
2	27.902	28.116	27.994	27.981
3	29.289	29.400	29.349	28.634
35	28.295	27.974	27.986	28.511
36	28.925	28.843	28.151	**26.931**
37	26.518	27.401	27.132	25.352
46	29.368	29.184	28.053	29.206
47	26.670	**28.439**	**28.072**	**28.712**
48	28.245	27.694	28.091	28.219
51	29.241	29.154	28.627	29.018
52	29.472	29.552	**29.007**	28.610
53	29.630	29.654	29.386	29.475
57	28.455	28.245	28.013	28.431
58	25.430	26.752	25.048	**28.148**
59	28.044	28.452	28.406	27.865
60	27.880	27.893	27.928	27.624
61	**27.862**	25.382	27.208	27.578
62	27.844	28.240	27.382	26.796
82	29.570	29.574	29.259	29.408
83	29.429	29.169	29.800	**29.269**
84	28.608	28.263	29.284	29.131

In Table 3, the bolded data represent the imputed values obtained through linear interpolation or extrapolation based on Equations 1 and 2. Once the missing data issue has been addressed, the dataset is ready for further analysis, including descriptive statistics, data exploration, and modeling using SARIMA, FFNN, and Hybrid SARIMA-FFNN.

Descriptive Statistics and Data Exploration

Table 4. Descriptive statistics.

Region	Min.	Max.	Mean	SD
North	25.061	30.355	28.517	1.239
East	24.956	30.241	28.448	1.237
South	24.942	30.200	28.438	1.231
West	24.941	30.231	28.469	1.180

Descriptive statistics were used to provide an overview of the characteristics of SST

data through the mean, minimum, maximum, and standard deviation values. Based on the results, it was observed that all values for each descriptive statistical measure across the regions were relatively similar. This indicates that the differences in SST among regions are not substantial. A complete descriptive statistical analysis for each location is presented in Table 4.

Based on Table 4, during the observation period on Enggano Island, the lowest recorded SST was in the western region at 24.941℃, while the highest SST was recorded in the northern region at 30.355℃. This indicates that SST on Enggano Island ranges from 24.941℃ to 30.355℃. Additionally, the average SST across all regions is approximately 28℃, with a standard deviation of 1℃. This suggests that the spatial variability of SST across the island is relatively low, indicating that SST in each region remained relatively stable throughout the observation period. The pattern of SST changes in each region over the observation period is visualized in Figure 3.

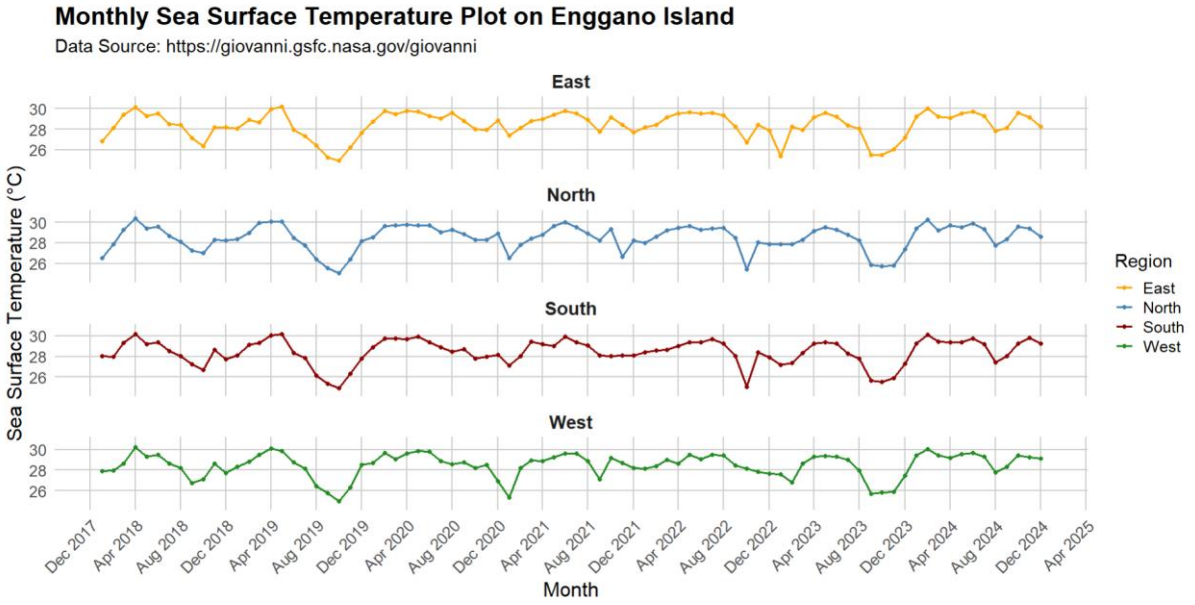

Figure 3. Plot of SST fluctuations on Enggano Island.

Based on Figure 3, it can be generally observed that SST across all regions of Enggano Island exhibits several periods of increase and decrease, with similar patterns of change. At a glance, recurring upward and downward fluctuations appear within certain time intervals. For instance, at the end of each year, SST in each region tends to show a noticeable decline. This provides an initial indication of the presence of seasonal patterns in SST across the regions of Enggano Island.

The seasonal pattern suggested by Figure 3 remains subjective, as it is based solely on visual observation. Therefore, seasonal pattern testing was conducted using spectral regression to identify the presence and strength of seasonal components statistically.

Seasonal Pattern Testing

For each region, testing was conducted under two data partitioning scenarios. First, assuming the presence of an annual seasonality, the data were divided into 72 training points and 12 testing points to preserve the full seasonal cycle. Second, to explore potential short-term seasonal patterns, such as quarterly or semiannual, a partitioning of 78 training points and 6 testing points was used. This partitioning aims to disrupt the annual cycle, allowing the identification of shorter seasonal

patterns, such as 3- or 6-month cycles. For example, Figure 4 presents a visualized periodogram plot for one of the regions. For other cases, periodogram plots can be visualized in the same manner.

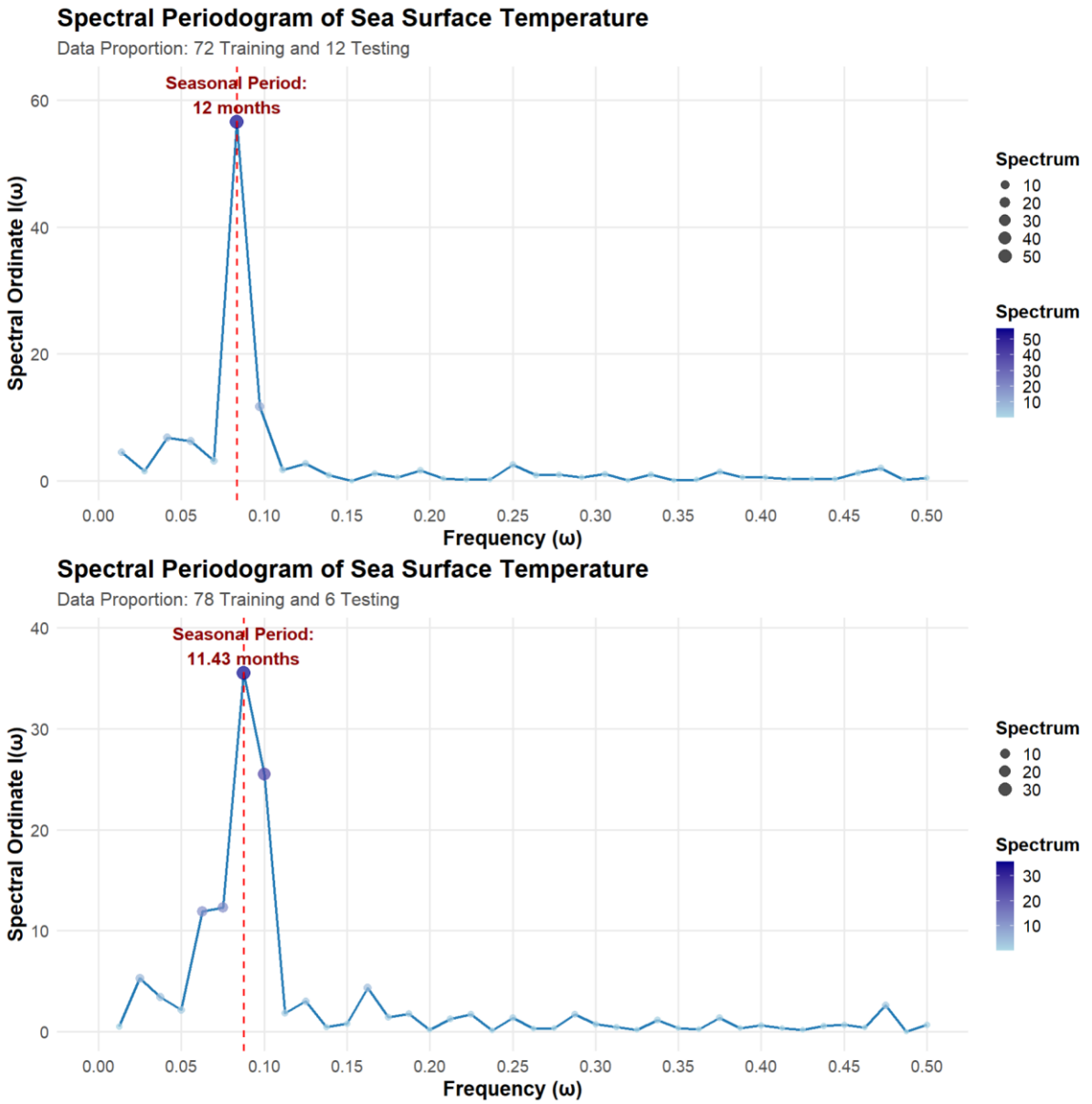

Figure 4. Periodogram plot of the Northern Region.

Table 5. Results of the seasonal component test.

Region	Period	$I(\omega_6)$	T	$g_{0.05}$
North	12	56.515	0.493	0.175
South	12	59.758	0.534	0.175
West	12	46.775	0.450	0.175
East	12	53.333	0.459	0.175

Based on the comparative test results of the two scenarios, it was observed that the training–testing data proportion of 72:12 consistently yielded higher ordinate values compared to the 78:6 proportion across all regions. For instance, as illustrated in Figure 4, the peak ordinate value obtained from the 72:12 proportion in the northern region was greater than that derived from the 78:6 proportion. This outcome suggests that employing a training period with an annual time interval is more effective in capturing the seasonal cycle, thereby facilitating a clearer identification of recurring patterns. Consequently, the seasonal

component identified under the 72:12 proportion was subjected to further analysis through spectral regression in order to statistically validate the existence, strength, and periodicity of the seasonal signal. The outcomes of this validation, including the statistical significance of the seasonal component, are summarized in Table 5. These findings provide a robust quantitative basis for characterizing the temporal structure of sea surface temperature variability around Enggano Island.

Based on Table 5, it can be observed that all regions have values $T > g_{0.05}$. This indicates that sea surface temperature across all regions of Enggano Island exhibits a annual seasonal pattern. Therefore, the sea surface temperature can be effectively modeled using the SARIMA approach.

Data Stationarity

Data stationarity is a prerequisite for SARIMA modeling and is tested through two assessments: stationarity with respect to variance and mean. The following presents the results of the stationarity check for variance.

Table 6. λ values in each region.

Trans.	λ			
	North	East	South	West
0	1.9999	1.9999	1.9999	1.9999
1	1.9999	1.9999	1.9999	1.9999
2	1.9999	1.9999	1.9999	1.9999
3	1.9999	1.9999	1.9999	1.9999
4	1.8404	1.7067	1.4163	1.5670
5	0.5321	1.2952	0.9086	0.8647
6	1.8766	1.0278	1.0518	1.0994

Based on the estimated λ parameters presented in Table 6, it can be observed that each region initially has a λ value of 1.9999. This indicates that the data are not yet variance-stationary. Therefore, a Box-Cox transformation in the form of $\frac{Z_t^{1.9999}-1}{1.9999}$ was applied. After applying the transformation up to three times, the λ value remained constant, suggesting that the Box-Cox transformation did not produce a significant change.

Considering that repeated transformations did not yield meaningful improvement and could potentially alter the data structure, increase model complexity, and complicate direct interpretation, the data were assumed to be variance-stationary, and subsequent analyses were conducted using the original data without Box-Cox transformation. This constitutes a limitation of the study.

Next, mean stationarity was assessed. The initial identification was conducted using ACF and PACF plots, which showed spikes in autocorrelation at certain lag multiples across all regions, indicating the presence of significant seasonal patterns. This aligns with the previous spectral regression analysis, which confirmed the existence of annual seasonal components. This pattern strongly suggests that the data do not satisfy the mean stationarity assumption, due to recurring seasonal fluctuations each year. Therefore, SST data in each region were addressed through seasonal differencing with a lag of 12. For example, Figure 5 presents the ACF and PACF plots of one region before and after the differencing process.

Based on Figure 5, it can be observed that after applying seasonal differencing, the previously dominant seasonal pattern appears weakened. This indicates that seasonal differencing successfully stabilized the seasonal mean. As a next step, the seasonally differenced data were tested for mean stationarity using the Augmented Dickey-Fuller (ADF) test. The results of the ADF test are presented in Table 7.

Table 7. Results of the ADF test.

Region	τ	$DF_{(0.05)}$	$P_{value}(\tau)$
North	-3.237	-1.95	0.002
East	-3.081	-1.95	0.003
South	-3.114	-1.95	0.003
West	-3.605	-1.95	0.001

Based on the results presented in Table 7, all regions have values $\tau < DF_{(0.05)}$ or

$P_{value}(\tau) < \alpha$. This indicates that the sea surface temperature data on Enggano Island satisfy the mean stationarity assumption. Once the stationarity test is confirmed, the analysis can proceed to SARIMA modeling.

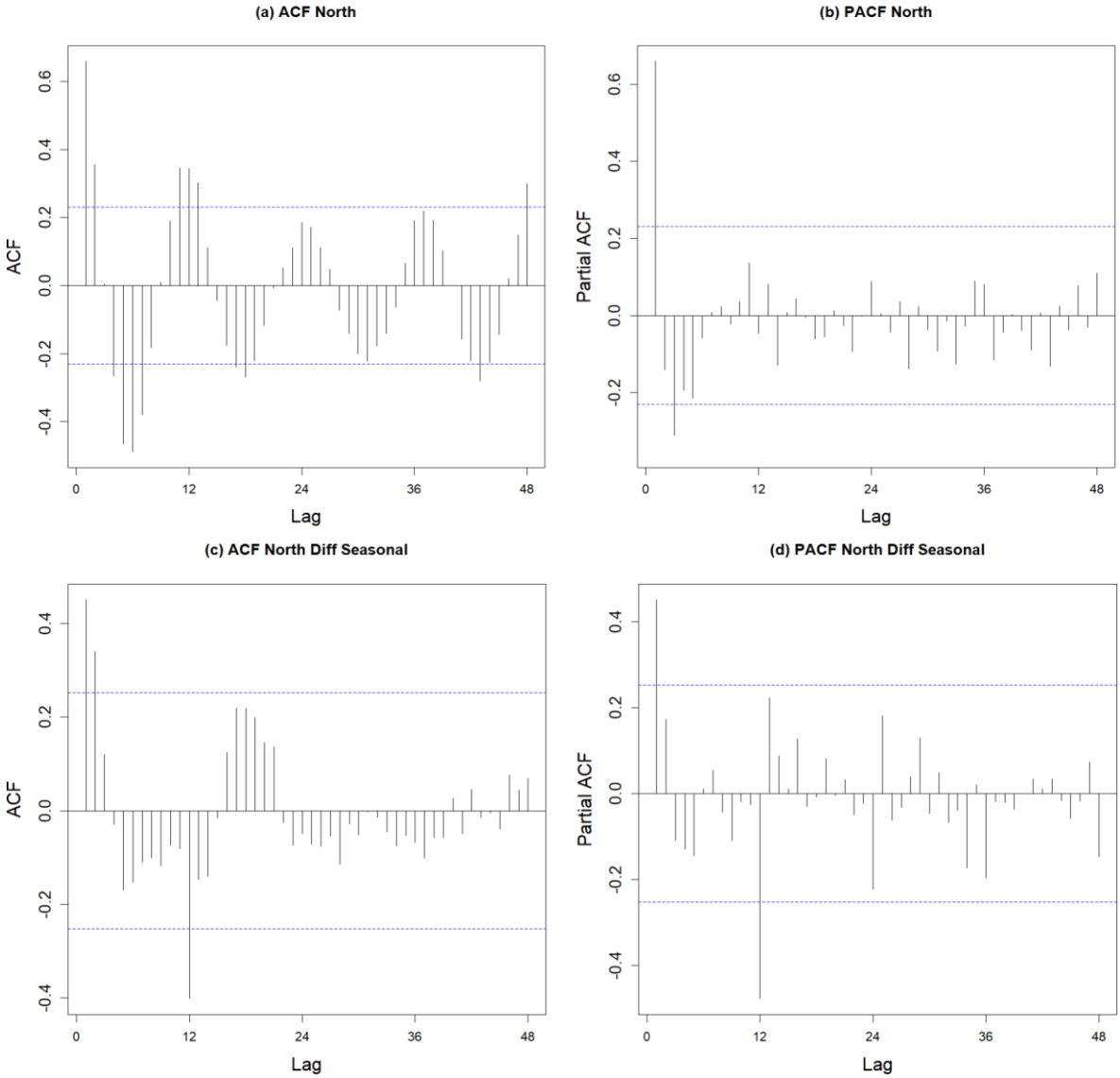

Figure 5. ACF and PACF plots of the Northern Region.

SARIMA Modeling

Table 8. Best SARIMA models.

Reg.	Model	Parameters	Estimates	Diagnostic Models					
				Ljung Box			KS		
				Q	$\chi^2_{\alpha;l}$	P_{value} (Q)	D_{KS}	$D_{\alpha;n}$	P_{value} (D_{KS})
North	SARIMA $(1,0,0)(0,1,1)^{12}$	AR(1) SMA(1)	0.547 -1	0.308	3.841	0.579	0.144	0.172	0.090
East	SARIMA $(1,0,0)(0,1,1)^{12}$	AR(1) SMA(1)	0.628 -1	0.012	3.841	0.912	0.144	0.172	0.091
South	SARIMA $(1,0,0)(0,1,1)^{12}$	AR(1) SMA(1)	0.587 -1	0.002	3.841	0.967	0.138	0.172	0.115
West	SARIMA $(1,0,0)(0,1,0)^{12}$	AR(1)	0.579	0.843	3.841	0.359	0.099	0.172	0.451

SARIMA modeling was conducted through a series of steps, including model identification using ACF and PACF plots, parameter estimation, parameter significance testing, model diagnostics, and selection of the best model. These steps produced the best SARIMA model for each region, as presented in Table 8, which lists the optimal model parameters alongside the results of diagnostic tests verifying model assumptions, such as residual autocorrelation and normality.

Based on Table 8, it can be seen that the best model for each region satisfies the model diagnostic assumptions, specifically regarding residual autocorrelation and normality. This is indicated by $P_{values}(Q \text{ and } D_{KS})$ greater than the chosen significance level (α). The fulfillment of these diagnostics suggests that the model adequately captures the underlying structure of the data, the residuals behave like white noise, and the parameter estimates are reliable for forecasting purposes.

The mathematical equations of the obtained models are as follows:

North

$$\hat{Z}_t = Z_{t-12} + 0.5472\, Z_{t-1} - 0.5472\, Z_{t-13} + e_t + e_{t-12}.$$

East

$$\hat{Z}_t = Z_{t-12} + 0.628 Z_{t-1} - 0.628 Z_{t-13} + e_{t-12} + e_t.$$

South

$$\hat{Z}_t = Z_{t-12} + 0.571 Z_{t-1} - 0.571 Z_{t-13} + e_{t-12} + e_t.$$

West

$$\hat{Z}_t = Z_{t-12} + 0.5792\, Z_{t-1} - 0.5792\, Z_{t-13} + e_t.$$

As an example, the following provides an interpretation of the SARIMA model for the western region of Enggano Island. Interpretations for other regions can be conducted in a similar manner.

The current sea surface temperature (SST) in the western region of Enggano Island is influenced by the SST of the previous month (lag 1), the SST of one year earlier (lag 12), and the SST of thirteen months earlier (lag 13).

1. An increase of 1℃ in the SST of the previous month (Z_{t-1}) increases the current SST by 0.5792℃, assuming other factors remain constant.
2. Conversely, an increase of 1℃ in the SST of thirteen months earlier (Z_{t-13}) decreases the current SST by 0.5792℃.
3. The SST of twelve months earlier (Z_{t-12}) directly contributes to the current SST with a coefficient of 1. This indicates that the SST of the same month in the previous year serves as the main baseline determining the current SST. In other words, the annual SST cycle in the western region is very strong and reflects a carry-over effect from the previous year.
4. In addition to these lagged effects, the current SST is also influenced by the error component (e_t), which represents random factors or external disturbances not captured by the model structure. This component reflects the inherent variability of SST that is unpredictable, such as short-term climatic events or weather anomalies.

Feed Forward Neural Network

Several steps were followed to model sea surface temperature using FFNN. The first step involved constructing the input data and normalizing it using min-max scaling. This study utilized monthly sea surface temperature data, resulting in 12 input neurons ($X_1, X_2, \ldots, X_{12}$) to fully represent the annual sequence of the time series, with each neuron reflecting the value from the preceding period.

Next, the FFNN architecture was designed, including the determination of the number of

neurons in the hidden layer, threshold values, and learning rate. In this study, the threshold was set at 0.1 to ensure that the training process would stop when the maximum weight gradient change was below 0.1. The learning rate was varied between 0.01 and 0.1, with increments of 0.01. The number of hidden neurons was then determined based on the configuration that produced the best evaluation metrics at the optimal learning rate. The resulting network architecture is presented in Table 9.

After obtaining the best network architecture for each region, the next step involved network training. This process included initializing weights and biases, followed by training using the backpropagation algorithm to obtain the optimal weights and biases. For illustration, Figure 6 presents one example of the resulting network architecture.

Table 9. Network architecture design.

Reg.	LR	Hidden Neurons	Network Architecture
North	0.01	2	FFNN (12-2-1)
East	0.07	9	FFNN (12-9-1)
South	0.01	2	FFNN (12-2-1)
West	0.03	2	FFNN (12-2-1)

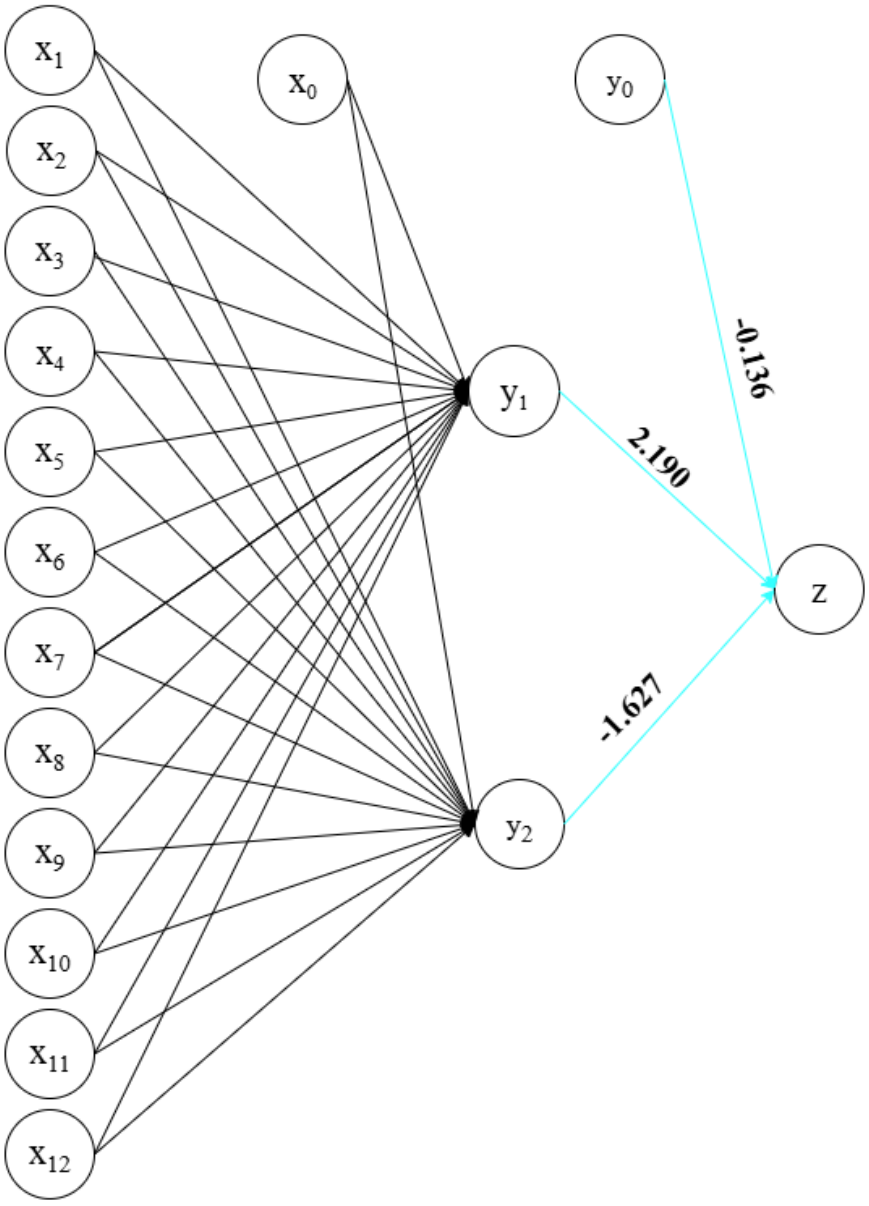

Figure 6. FFNN (12-2-1) Network architecture for the Northern Region of Enggano Island.

Based on Figure 6, the architecture of the FFNN network follows a (12-2-1) structure, consisting of 12 input neurons ($X_1, \dots, X_{12}$), 2 hidden neurons (y_1, y_2), and 1 output neuron (z_1). Each input neuron and bias is fully connected to all hidden neurons. The relationship between the input layer and the hidden layer is represented by the weights v_{ih}. Subsequently, each hidden neuron transmits its nonlinear activation to the output neuron through the weights w_{hr}.

The training results of the network for all regions can be expressed mathematically as follows:

North

$$\hat{Z}_t = f\Big((-0.136) + \big((y_1)(2.190)\big) + \big((y_2)(-1.627)\big)\Big).$$

East

$$\hat{Z}_t = f((-0.443) + \big((y_1)(0.209)\big) + \big((y_2)(-1.074)\big) + \big((y_3)(0.094)\big) + \big((y_4)(-1.157)\big) + \big((y_5)(-1.115)\big) + \big((y_6)(0.690)\big) + \big((y_7)(2.352)\big) + \big((y_8)(-0.364)\big) + \big((y_9)(0.274)\big).$$

South

$$\hat{Z}_t = f((0.007) + \big((y_1)(2.162)\big) + \big((y_2)(-1.774)\big)$$

West

$$\hat{Z}_t = f((0.609) + \big((y_1)(0.074)\big) + \big((y_2)(-1.147)\big).$$

As an example, the following provides an interpretation of the FFNN model for the northern region of Enggano Island. Interpretations for other regions can be conducted in a similar manner.

1. The current SST in the western region of Enggano Island is influenced by a nonlinear combination of two hidden neurons (y_1 and y_2) that are derived from transformations of the input variables (lagged SST values). The contribution of each hidden neuron to the current SST is represented by the output layer weights, with a value of 2.190 for neuron y_1 and –1.627 for neuron y_2. This indicates that the activation of neuron y_1 positively amplifies the current SST, while the activation of neuron y_2 contributes negatively, thereby reducing the current SST.
2. In addition, there is a bias of –0.136, which functions as a constant in the model to adjust the predictions and better align them with the observed data patterns.

Thus, the FFNN model captures more complex and nonlinear relationships among the lagged SST values compared to a linear model such as SARIMA. The hidden neurons y_1 and 2 serve as transformation functions that filter patterns from historical data, which are then combined in the output layer to predict the current SST.

Hybrid SARIMA-FFNN

Table 10. Network architecture design.

Reg.	LR	Network Architecture
North	0.1	*Hybrid* (SARIMA(1,0,0)(0,1,1)^{12}-FFNN (12-10-1))
East	0.01	*Hybrid* (SARIMA(1,0,0)(0,1,1)^{12}-FFNN (12-5-1))
South	0.01	*Hybrid* (SARIMA(1,0,0)(0,1,1)^{12}-FFNN (12-5-1))
West	0.02	*Hybrid* (SARIMA(1,0,0)(0,1,0)^{12}-FFNN (12-5-1))

In the Hybrid SARIMA-FFNN modeling, the input data consist of the errors from the best SARIMA model in each region. These errors are modeled using the FFNN mechanism to capture and learn the nonlinear patterns within them. The predicted errors are then added to the predictions from the SARIMA model to obtain improved overall forecasts. The resulting network architecture design for each region is presented in Table 10.

The results of network training across all regions can be mathematically represented as follows:

$$\hat{Z}_t = \hat{Z}_t^{(L)} + \hat{Z}_t^{(NL)}.$$

North

$$\hat{Z}_t^{(L)} = Z_{t-12} + 0.5472\, Z_{t-1} - 0.5472\, Z_{t-13} + e_t + e_{t-12}.$$

$$\hat{Z}_t^{(NL)} = f((5.435) + ((y_1)(5.031)) + ((y_2)(2.008)) + ((y_3)(-3.221)) + ((y_4)(-4.899)) + ((y_5)(-4.995)) + ((y_6)(-2.076)) + ((y_7)(-2.308)) + ((y_8)(3.754)) + ((y_9)(-4.888)) + ((y_{10})(4.394)).$$

East

$$\hat{Z}_t^{(L)} = Z_{t-12} + 0.628Z_{t-1} - 0.628Z_{t-13} + e_{t-12} + e_t.$$

$$\hat{Z}_t^{(NL)} = f((-0.276) + ((y_1)(0.047)) + ((y_2)(0.019)) + ((y_3)(0.376)) + ((y_4)(1.861)) + ((y_5)(-0.748)).$$

South

$$\hat{Z}_t^{(L)} = Z_{t-12} + 0.571Z_{t-1} - 0.571Z_{t-13} + e_{t-12} + e_t.$$

$$\hat{Z}_t^{(NL)} = f((-0.224) + ((y_1)(0.065)) + ((y_2)(0.028)) + ((y_3)(0.422)) + ((y_4)(1.871)) + ((y_5)(-0.731)).$$

West

$$\hat{Z}_t^{(L)} = Z_{t-12} + 0.5792\, Z_{t-1} - 0.5792\, Z_{t-13} + e_t.$$

$$\hat{Z}_t^{(NL)} = f((-0.216) + ((y_1)(0.063)) + ((y_2)(0.027)) + ((y_3)(0.426)) + ((y_4)(1.888)) + ((y_5)(-0.747)).$$

As an example, the following provides an interpretation of the Hybrid SARIMA-FFNN model for the eastern region of Enggano Island.

1. Interpretations of each model component separately (SARIMA and FFNN) can be conducted as previously described.
2. In general, the Hybrid model predicts SST by combining linear predictions from SARIMA with nonlinear predictions from FFNN. In the FFNN stage, the model processes the residuals or errors from the SARIMA model, allowing the FFNN to capture nonlinear patterns not explained by SARIMA. The final SST prediction is obtained by summing the SARIMA forecast and the FFNN output, enabling the Hybrid model to account for both linear seasonal patterns and more complex nonlinear dynamics.
3. The FFNN consists of one hidden layer with five neurons $(y_1, y_2, y_3, y_4, y_5)$. The output weights of these neurons are 0.047, 0.019, 0.376, 1.861, and –0.748, with a bias of –0.276. Each neuron processes the SARIMA residuals to extract nonlinear patterns:
   a. Neurons with positive weights (y_1, y_2, y_3, y_4) amplify the SST prediction,
   b. Neurons with negative weights (y_5) reduce the SST prediction.

Thus, the FFNN acts as a transformation function that filters the SARIMA residuals to capture nonlinear interactions among lagged SST values, before combining them in the output layer to produce the final SST forecast.

Selection of the Best Method for Each Region

The best method was determined by comparing the predictive performance of the three methods in each observation region. The following presents a visualization of the comparison between predicted results and actual testing data for each region.

Figures 7 to 10 present comparative plots between the actual data and the prediction results of the testing dataset across all methods in each region. In these plots, the red line represents the actual data, while the blue line represents the predicted values. As

shown in Figure 7, the SARIMA model in the northern region of Enggano demonstrates a relatively better predictive performance in capturing the actual data patterns compared to the FFNN and Hybrid SARIMA-FFNN models. Conversely, as illustrated in Figures 8 to 10, the FFNN model appears to follow the actual data patterns more closely than SARIMA and Hybrid SARIMA-FFNN in the eastern, southern, and western regions.

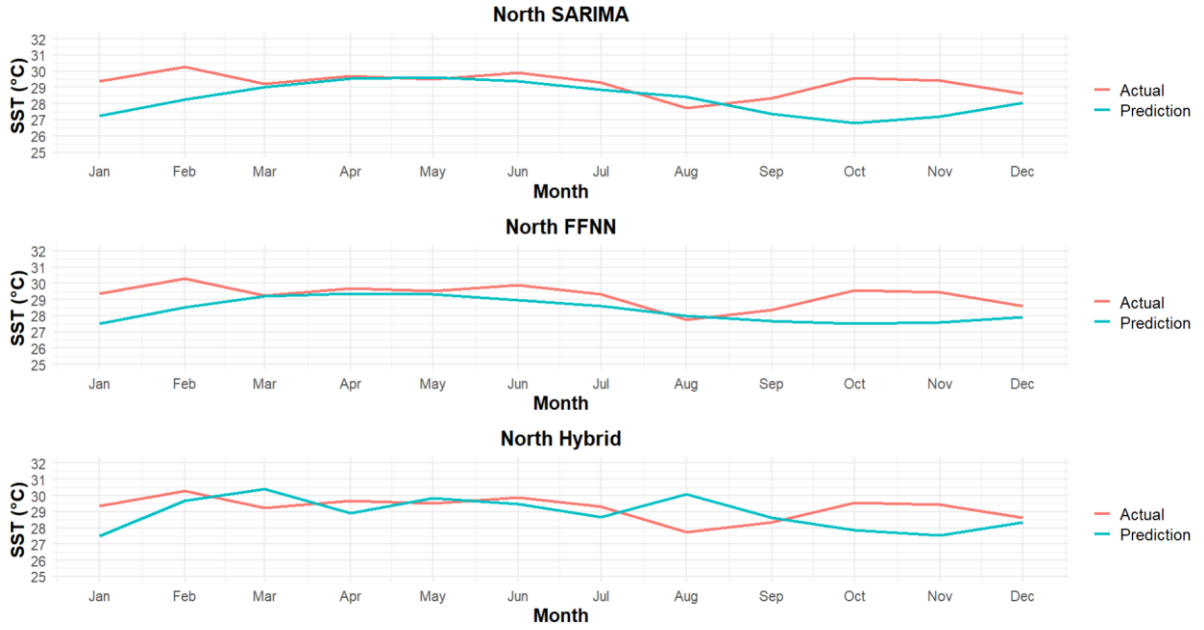

Figure 7. Plot of the model prediction results for Enggano's northern region.

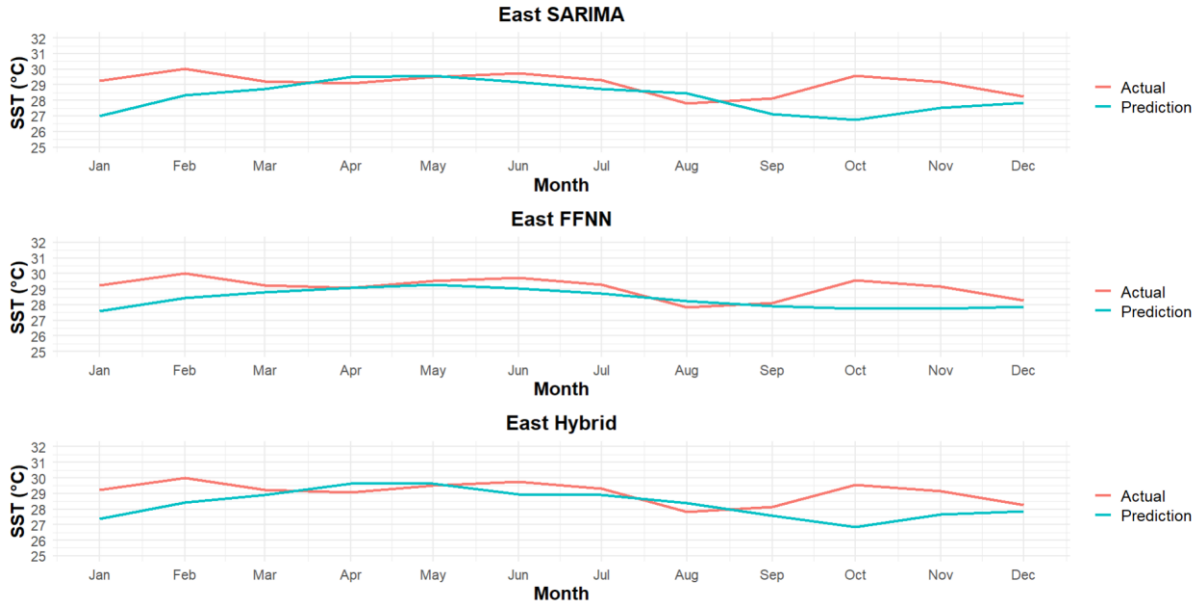

Figure 8. Plot of the model prediction results for Enggano's eastern region.

It should be noted that determining the best-performing method based solely on visual inspection of the comparative plots is inherently subjective and may not guarantee accuracy at each individual data point. Consequently, the selection of the optimal method in each region is more appropriately determined objectively using the lowest RMSE value derived from the prediction results on the testing dataset. The evaluation results are summarized in Table 11.

Table 11. Prediction evaluation results.

Model	North		East		South		West	
	RMSE	MAPE	RMSE	MAPE	RMSE	MAPE	RMSE	MAPE
SARIMA	1.409	3.652	1.330	3.597	1.404	3.778	2.040	5.270
FFNN	1.173	3.188	0.999	2.691	1.245	3.465	1.049	3.304
Hybrid SARIMA-FFNN	1.245	3.526	1.212	3.240	1.342	3.512	1.984	5.198

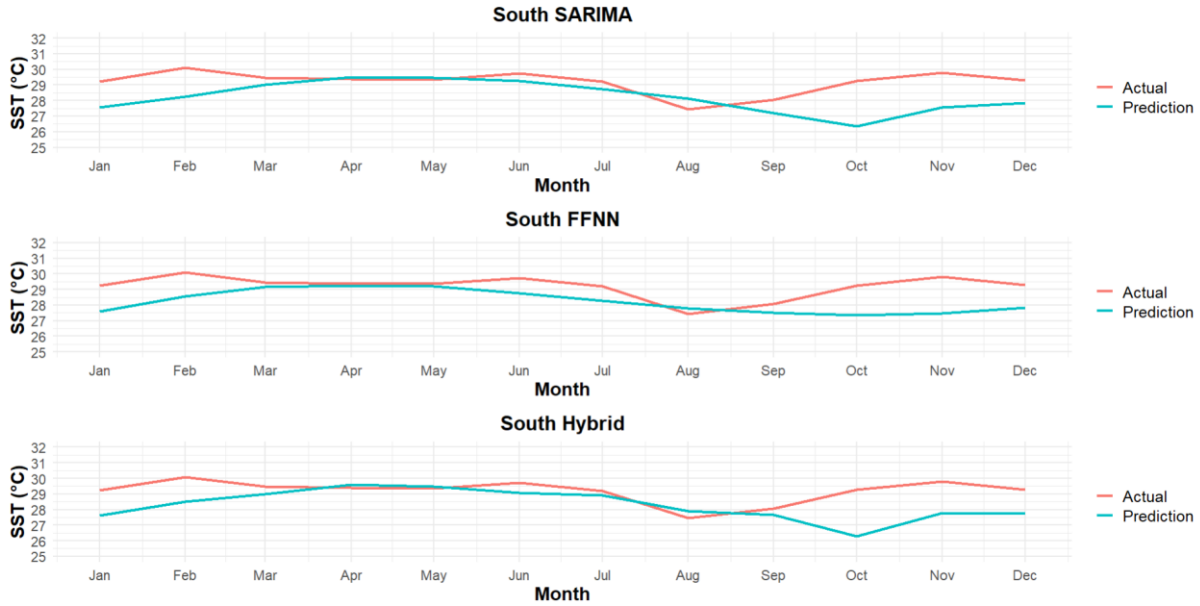

Figure 9. Plot of the model prediction results for Enggano's southern region.

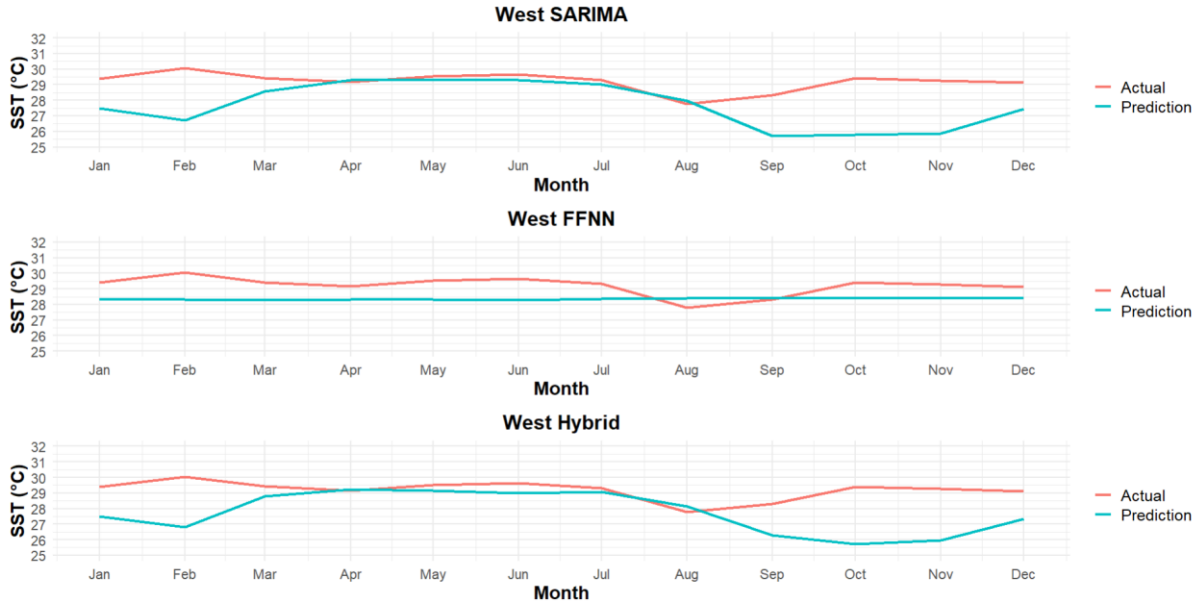

Figure 10. Plot of the model prediction results for Enggano's western region.

Based on Table 11, it can be seen that all models in the sea surface temperature modeling across Enggano Island demonstrate very high predictive performance. This is indicated by the MAPE values for each model in all regions being below 10%. Based on the RMSE values, it is evident that the Hybrid SARIMA-FFNN model consistently improves prediction accuracy compared to the standalone SARIMA model in all regions. However, the Hybrid SARIMA-FFNN model has not yet been able to surpass the performance of the FFNN model. This is reflected in the evaluation results, which show that FFNN is the best-performing model across all observation areas. This indicates that

the sea surface temperature data in Enggano Island is more suitably modeled using a nonlinear approach, specifically FFNN.

After it was determined that the FFNN model with each of its architectures is the best model across all regions, the model was then used to predict sea surface temperature. The prediction results are presented in Table 12.

Based on the prediction results presented in Table 12, it can be observed that the predicted values across the four regions for each month exhibit only minor differences. The predicted SST values fall within the range of 27.340℃ to 29.628℃. This temperature range is within the optimal conditions preferred by pelagic fish, which are between 26℃ and 29℃ (Esra et al., 2023). Meanwhile, other fish species may require adjustments according to their respective temperature preferences. The relatively similar SST predictions across regions provide greater flexibility for fishermen to conduct fishing activities without being constrained by regional differences. Nevertheless, adjustments must still be made based on the temperature preferences of the targeted fish species, as well as considering other factors that influence fish distribution.

Table 12. Prediction results of SST.

Month	North	East	South	West
January	27.528	27.610	27.611	28.341
February	28.509	28.419	28.574	28.300
March	29.191	28.807	29.157	28.272
April	29.368	29.099	29.265	28.314
May	29.327	29.278	29.202	28.328
June	28.971	29.033	28.752	28.282
July	28.596	28.728	28.293	28.355
August	27.979	28.243	27.779	28.382
September	27.692	27.896	27.522	28.397
October	27.522	27.754	27.340	28.404
November	27.607	27.754	27.451	28.391
December	27.905	27.882	27.830	28.386

Conclusion

The sea surface temperature (SST) in Enggano Island exhibits a relatively low spatial variability across the region, indicating that SST in each area remained relatively stable throughout the observed period. The optimal model for predicting sea surface temperature across all regions of Enggano Island for 2018–2024 was the FFNN. The details of the best network architecture are as follows: in the northern region, FFNN(12-2-1); in the eastern region, FFNN(12-9-1); in the southern region, FFNN(12-2-1); and in the western region, FFNN(12-2-1).

Based on the evaluation of model predictive performance using RMSE and MAPE values, all models for SST prediction in Enggano Island demonstrated very high predictive accuracy across all regions. This is indicated by MAPE values below 10% for each model in all areas. The most effective approach for modeling SST was the FFNN, with the best-performing architectures as follows: in the northern region, FFNN(12-2-1) with an RMSE of 1.173; in the eastern region, FFNN(12-9-1) with an RMSE of 0.999; in the southern region, FFNN(12-2-1) with an RMSE of 1.245; and in the western region, FFNN(12-2-1) with an RMSE of 1.049.

Based on the prediction results, the relatively consistent SST enables fishermen to carry out fishing activities more flexibly, without the need to consider regional differences. However, fishing practices should be adjusted according to the preferred temperature ranges of the target fish species, and other factors that influence fish distribution should be taken into account.

A limitation of this study is the violation of the variance stationarity assumption. Theoretically, this may result in biased SARIMA parameter estimates and inaccurate inferences (Ryan et al., 2025). Nevertheless, the study's findings indicate that, despite this violation, the model's predictions for the testing data across all regions still exhibited very high performance. This suggests that, in certain contexts, violating the variance stationarity

assumption does not necessarily hinder a model's ability to generate effective predictions. However, further research is recommended using alternative models that can address this issue, in order to achieve improved results and enhance the reliability of SST information to support fishing activities on Enggano Island.

Acknowledgements

The authors would like to express their gratitude to the NASA Goddard Earth Sciences Data and Information Services Center (GES DISC) through the Giovanni platform for facilitating the provision of sea surface temperature data, which served as the basis for this study's analysis.

The authors also extend their sincere appreciation to the editor, reviewers, and proofreader for their valuable contributions and suggestions that helped improve this manuscript. Special thanks are conveyed to the research team at the Department of Statistics, Faculty of Mathematics and Natural Sciences, University of Bengkulu, for their support in preparing equipment, data collection, and analysis throughout this study.

Author Contribution

Raditya Janaloka Natisharevi: Conceptualization, Methodology, Data Curation, Formal Analysis, Software, Writing – Original Draft. Conducted the research, collected SST data, implemented SARIMA, FFNN, and Hybrid SARIMA-FFNN modeling in R, and drafted the manuscript.

Jose Rizal: Supervision, Conceptualization, Writing – Review and Editing. Provided guidance on research design, methodology, and data analysis.

Firdaus: Validation, Formal Analysis, Writing – Review and Editing. Assisted in data analysis and validation, providing academic insights.

Pepi Novianti: Provided input during the data cleaning process to ensure the integrity of the processed data. Offered new perspectives in data interpretation and ensured the accuracy of the analysis in accordance with the research objectives.

Wina Ayu Lestari: Writing – Review and Editing, Supervision. Evaluated research findings, advised on FFNN training, and recommended improvements to the analysis.

Conflict of Interest

All authors have reviewed and approved this manuscript. The authors affirm that this article is an original work, is not under consideration by any other journal, and that there are no conflicts of interest. All stages of the research, analysis, and manuscript preparation were conducted independently and objectively, without influence from any external party.

References

Alrowais, R., Alwushayh, B., Bashir, M. T., Nasef, B. M., Ghazy, A., & Elkamhawy, E. (2023). Modeling and Analysis of Cutoff Wall Performance Beneath Water Structures by Feed-Forward Neural Network (FFNN). *Water*, 15(21), 3870. https://doi.org/10.3390/w15213870

Aminy, L. N., & Walid, W. (2022). Perbandingan Model Feed Forward Neural Network dan Arima untuk Meramalkan Perkembangan Covid-19 di Indonesia. *MATHunesa Jurnal Ilmiah Matematika*, 12(1), 1–10. https://doi.org/10.26740/mathunesa.v12n1.p1-10

Azmi, B. N., Hermawan, A., & Avianto, D. (2023). Analisis Pengaruh Komposisi Data Training dan Data Testing pada Penggunaan PCA dan Algoritma Decision Tree untuk Klasifikasi Penderita Penyakit Liver. *JTIM : Jurnal Teknologi Informasi dan Multimedia*, 4(4), 281–290. https://doi.org/10.35746/jtim.v4i4.298

Baharudin, A., Tangke, U., & Titaheluw, S. S. (2022). Distribusi Parameter Oseanografi Dengan Hasil Tangkapan

Ikan Pelagis Kecil Untuk Pemetaan Distribusi Daerah Potensial Penangkapan Di Perairan Teluk Weda. *Jurnal Biosainstek*, 4(1), 32–41. https://jurnal.ummu.ac.id/index.php/biosaintek/article/view/719

Chicco, D., Warrens, M. J., & Jurman, G. (2021). The Coefficient of Determination R-squared is More Informative than SMAPE, MAE, MAPE, MSE and RMSE in Regression Analysis Evaluation. *PeerJ Computer Science*, 7, e623. https://doi.org/10.7717/peerj-cs.623

Crayer, J. D. & Chan, K.-S. (2008). *Time Series Analysis with Applications in R*. Springer Science+Business Media. 2 ed. New York. https://doi.org/10.1007/978-0-387-75959-3

Esra, G., Herliany, N. E., & Adriani, A. (2023). Analisis Spasial Dna Temporal Hasil Tangkapan Ikan Pelagis Dan Thermal Front pada Musim Peralihan di Kabupaten Toli-Toli Sulawesi Tengah. *Prosiding Seminar Nasional Hasil Penelitian Kelautan Dan Perikanan*, 1(1), 147–152. https://semnas.bpfp-unib.com/index.php/semnaskel/article/view/115

Fadhlia, S., Hendri, E. P., & Cahyaningtyas A, D. D. (2024). Model Peramalan Nilai Tukar Rupiah Terhadap Dollar Singapura Menggunakan Metode Hybrid ARIMA-ANN. *Jurnal Ilmiah Pendidikan Matematika, Matematika Dan Statistika*, 5(3), 1513–1523. https://doi.org/10.46306/lb.v5i3.720

Glorot, X., & Bengio, Y. (2010). Understanding the Difficulty of Training Deep Feedforward Neural Networks. *Journal of Machine Learning Research*, 9, 249–256. https://proceedings.mlr.press/v9/glorot10a.html

Hastuti, R. P. W., Widianingsih, W., & Nuraini, R. A. T. (2024). Kondisi Meteorologi Laut Terhadap Suhu Permukaan Laut Di Perairan Kota Surabaya Tahun 2019 – 2021. *Journal of Marine Research*, 13(4), 701–712. https://doi.org/10.14710/jmr.v13i4.43227

Hisyam, M., Sumardi, S. R., Kainama, T. L. J., & Haryati, K. (2025). Prediksi Suhu Permukaan Laut di Perairan Kota Jayapura Tahun 2021-2025 Menggunakan Model SARIMA. *ACROPORA: Jurnal Ilmu Kelautan Dan Perikanan Papua*, 8(1), 37–43. https://doi.org/10.31957/acr.v8i1.4605

Ichwan, M., & Alfarisyi, S. F. (2024). Pemodelan Ritme Kalori Terbakar Setiap Waktu Selama Bersepeda dengan Feedforward Neural Network. *ELKOMIKA: Jurnal Teknik Energi Elektrik, Teknik Telekomunikasi, & Teknik Elektronika*, 12(1), 13–22. https://doi.org/10.26760/elkomika.v12i1.13

Izonin, I., Tkachenko, R., Shakhovska, N., Ilchyshyn, B., & Singh, K. K. (2022). A Two-Step Data Normalization Approach for Improving Classification Accuracy in the Medical Diagnosis Domain. *Mathematics*, 10(11), 1942. https://doi.org/10.3390/math10111942

Kambey, E. M., Jasin, M. I., & Mamoto, J. D. (2023). Studi Hidro Oseanografi Di Pantai Ranowulu. *Tekno*, 21(83), 319–326. https://ejournal.unsrat.ac.id/v3/index.php/tekno/article/view/47332

Kurniasari, D., Mahyunis, R. V., Warsono, W., & Nuryaman, A. (2023). Implementation of Artificial Neural Network (ANN) Using Backpropagation Algorithm By Comparing Four Activation Functions in Predicting Gold Prices. *Kumpulan Jurnal Ilmu Komputer (KLIK)*, 10(1), 93–105. https://klik.ulm.ac.id/index.php/klik/article/view/587

Li, M. (2024). Comprehensive Review of

Backpropagation Neural Networks. *Academic Journal of Science and Technology*, 9(1), 150–154. https://doi.org/10.54097/51y16r47

NASA Goddard Earth Sciences Data and Information Services Center (GES DISC). (2024). Giovanni Interactive Visualization and Analysis. *NASA GES DISC*. https://giovanni.gsfc.nasa.gov/giovanni

Pangruruk, F. A., & Barus, S. P. (2022). Predicting the Number of People Exposed to Covid 19 with the Newton Gregory Maju Polynomial Interpolation Method. *Formosa Journal of Science and Technology*, 1(8), 1275–1290. https://doi.org/10.55927/fjst.v1i8.2185

Permana, I., & Salisah, F. N. (2022). The Effect of Data Normalization on the Performance of the Classification Results of the Backpropagation Algorithm Pengaruh Normalisasi Data Terhadap Performa Hasil Klasifikasi Algoritma Backpropagation. *Indonesian Journal of Informatic Research and Software Engineering*, 2(1), 67–72. https://doi.org/10.57152/ijirse.v2i1.311

Puteri, D. I. (2023). Implementasi Long Short Term Memory (LSTM) dan Bidirectional Long Short Term Memory (BiLSTM) Dalam Prediksi Harga Saham Syariah. *Euler : Jurnal Ilmiah Matematika, Sains Dan Teknologi*, 11(1), 35–43. https://doi.org/10.34312/euler.v11i1.19791

Rifai, S. N. (2023). Analisis Oseanografi Lautan Menggunakan Model Jaringan Syaraf Tiruan. *Prosiding Seminar Nasional Pemanfaatan Sains Dan Teknologi Informasi*, 1(1), 1–10. https://epublikasi.digitallinnovation.com/index.php/sempatin/article/view/35

Ryan, O., Haslbeck, J. M. B., & Waldorp, L. J. (2025). Non-Stationarity in Time-Series Analysis : Modeling Stochastic and Deterministic Trends. *Multivariate Behavioral Research*, 60(3), 556–588. https://doi.org/10.1080/00273171.2024.2436413

Sari, I. P. (2020). Agama, Etnisitas dan Perdamaian di Pulau Enggano Provinsi Bengkulu. Hanifiya: Jurnal Studi Agama-Agama, 3(2), 77–86. https://doi.org/10.15575/hanifiya.v3i2.9987

Septiana, D., & Bangun, M. B. (2023). Perbandingan Antara Feed Forward Neural Network (FFNN) Dan Seasonal Autoregressive Integrated Moving Average (Sarima) Untuk Peramalan Data Runtun Waktu Terapan. *Jurnal Deli Sains Informatika*, 2(2). https://jurnal.unds.ac.id/index.php/dsi/article/view/218

Shabrina, N. N., Sunarto, S., & Hamdani, H. (2017). Penentuan Daerah Penangkapan Ikan Tongkol Berdasarkan Pendekatan Distribusi Suhu Permukaan Laut dan Hasil Tangkapan Ikan di Perairan Utara Indramayu Jawa Barat. *Jurnal Perikanan Dan Kelautan*, 8(1), 139–145. https://jurnal.unpad.ac.id/jpk/article/view/13901

Silsia, D., Yahya, R., & Lumbanbatu, U. M. (2019). Rendemen dan Karakteristik Minyak Bintangur dari Pulau Enggano Sebagai Bahan Baku Pembuatan Biodiesel. *Jurnal Agroindustri*, 9(1), 1–7. https://doi.org/10.25077/greentech.v1i1.10

Susila, M. R., Jamil, M., & Santoso, B. H. (2023). Akurasi Model Hybrid ARIMA-Artificial Neural Network dengan Model Non Hybrid pada Peramalan Peredaran Uang Elektronik di Indonesia. *Jambura Journal of Mathematics*, 5(1), 46–58. https://doi.org/10.34312/jjom.v5i1.14889

Syahrin, K. A., Disera, T. E., Youwea, A.

S. G. N., Merdeka, J., Saputra, A. H., Norman, Y., & Nugraheni, I. R. (2024). Prakiraan Perubahan Suhu Permukaan Laut dengan Neuralprophet di Taman Laut Bunaken. *Jurnal Laut Pulau*, 3(2), 42–50. https://doi.org/10.30598/jlpvol3iss2pp42-50

Wei, W. W. S. (2006). *Time Series Analysis Univariate and Multivariate Methods* (2nd ed.), Pearson. https://civil.colorado.edu/~balajir/CVEN6833/lectures/wwts-book.pdf

Wulandari, S., & Novita, D. (2024). Implementasi Feed Forward Neural Network (FFNN) dalam Memprediksi Penyakit Diabetes. *Jurnal MIPA Sains Terapan*, 3(1), 1–11. https://journal.unindra.ac.id/index.php/sainsmath/article/view/3048

Zhang, G. P. (2003). Time series forecasting using a hybrid ARIMA and neural network model. *Neurocomputing*, 50, 159–175. https://doi.org/10.1016/S0925-2312(01)00702-0

Zhang, Y., & Meng, G. (2023). Simulation of an Adaptive Model Based on AIC and BIC ARIMA Predictions. *Journal of Physics: Conference Series*, 2449(1), 012027. https://doi.org/10.1088/1742-6596/2449/1/012027